

The impact of atmospheric stability and wind shear on vertical cloud overlap over the Tibetan Plateau

Jiming Li^{1,*}, Qiaoyi Lv², Bida Jian¹, Min Zhang¹,
Chuanfeng Zhao³, Qiang Fu^{1,4}, and Kazuaki Kawamoto⁵, Hua Zhang⁶

5

¹Key Laboratory for Semi-Arid Climate Change of the Ministry of Education, College of Atmospheric Sciences, Lanzhou University, Lanzhou, China

²Laboratory of Straits Meteorology, Xiamen Meteorological Bureau, Xiamen, China

³State Key Laboratory of Earth Surface Processes and Resource Ecology, and College of Global Change and Earth System Science, Beijing Normal University, Beijing, China

⁴Department of Atmospheric Sciences, University of Washington, Seattle, USA

⁵Graduate School of Fisheries and Environmental Sciences, Nagasaki University, Nagasaki, Japan

⁶Laboratory for Climate Studies, National Climate Center, China Meteorological Administration, Beijing, China

Corresponding author: Jiming Li, Key Laboratory for Semi-Arid Climate Change of the Ministry of Education, College of Atmospheric Sciences, Lanzhou University, Lanzhou, Gansu 730000, China. (lijiming@lzu.edu.cn)

Abstract

The accurate representation of cloud vertical overlap in atmospheric models is important for simulating the total cloud cover and the radiative energy budget in these models. However, this subject has received little attention due to the limited observation, especially over the Tibetan Plateau (TP), where has experienced a rapid climate warming over the past three decades. In this study, 4 years (2007–2010) of data from the CloudSat cloud product and collocated ERA-Interim reanalysis product are analyzed to examine the cloud overlaps over the TP region, and evaluate the effect

of atmospheric dynamic and thermodynamic environment on these cloud overlaps. The overlap parameter α and decorrelation length scale L , which are widely used to characterize the transition from the maximum to random overlap assumption with increasing layer separations, are calculated and discussed. It is confirmed that continuous cloud layers tend to have a maximum overlap at a small separation but gradually become randomly overlapped with increasing cloud layer separations. It is found that for the continuous cloud layers, the overlap parameter α is sensitive to the unique thermo-dynamic and dynamic environment over the TP, i.e., the unstable atmospheric stratification and corresponding weak wind shear, which leads to maximum overlap (that is, greater α values). This finding agrees well with the previous studies. We parameterize the decorrelation length scale L as a function of the wind shear and atmospheric stability based on a multiple linear regression. Compared with previous parameterizations, this new scheme improves the simulation of cloud cover over TP when the separations between cloud layers are larger than 1km. This study indicates that effects of both wind shear and atmospheric stability on cloud overlap should be taken into account in the parameterization of overlap parameter α to improve the simulation of total cloud cover in atmospheric models.

1. Introduction

Clouds strongly modulate the Earth's radiative energy budget, via changes in their macrophysical (e.g., cloud cover, height, and thickness) and microphysical properties (e.g., cloud water contents, phase and droplet and crystal size) (Rossow and Lacis, 1990; Hartmann et al., 1992; Fu and Liou, 1993; Fu et al., 2002; Stephens, 2005; Kawamoto and Suzuki, 2012; Yan et al., 2012; Wang et al., 2010). However, our incomplete understanding of their underlying physical processes makes the representation of clouds in climate models still unreliable, which keeps clouds as the largest uncertainty when estimating and interpreting changes in the Earth's energy budget (Boucher et al., 2013).

The Tibetan Plateau (TP), which is also known as the “roof of the world” or the “world water tower”, plays a significant role in determining global atmospheric circulations, in addition to its strong influence over Asia via its thermal-dynamic and dynamic forcings (Yanai et al., 1992; Ye and Wu, 1998; Duan and Wu, 2005; Xu et al., 2008; Wu et al., 2015). Over the past three decades (Kang et al., 2010), the TP has experienced distinct climate changes including the changes in atmospheric circulations and hydrological cycles (Yang et al., 2014). Many studies have showed that significant warming occurs in the TP region during the last decades and it will continue in the future (e.g., Duan et al., 2006; Wang et al., 2008). The rapid warming has caused glacier retreat and expansion of glacier-fed lakes (Zhu et al., 2010), permafrost degradation (Cheng and Wu, 2007), heating source has become weakened (Yang et al., 2011). The warming and weakened heating source also affects the summer precipitation downstream (Duan et al., 2013). In a review paper, Kang et al. (2010) summarized that the changes of cloud cover based on observations also is one of dominant factors causing the rapid warming over TP region in addition to increased greenhouse gas emission. Many studies indeed have linked the rapid warming over TP to changes in the cloud cover over the TP region (e.g., Chen and Liu, 2005; Duan and Wu, 2006; Li et al., 2006; Yang et al., 2012; You et al., 2014; Wu et al., 2014). A recent study has indicated that increased nocturnal cloud cover over the northern TP could increase the nighttime temperature by enhancing downward surface infrared

radiation, while decreased daytime cloud over the southern TP has contributed to the increase of surface air temperature during daytime by enhancing downward surface solar radiation (Duan and Xiao, 2015). Because of the importance of clouds in climate change, it is critically important to reliably represent the cloud cover and its relation to large-scale thermodynamic and dynamic conditions in the climate models in order to better predict the climate changes over TP.

However, our understanding about the role of cloud cover on the radiation balance and water cycle over the TP region remains poor because of the limited availability of regional cloud observations and our incomplete representation of the cloud physical processes in climate models. One of the remaining challenges involves how to reasonably represent the characteristics of the vertical overlapping of cloud layers in these models. Cloud overlap means that two or more cloud layers are simultaneously present over the same location but at different levels in the atmosphere. It is usually defined in terms of three basic overlap assumptions: maximum, random and minimum.

If the cloud cover in two model layers is given by C_i and C_j , respectively, total cloud cover of any two cloud layers from maximum assumption is $C_{i,j}^{\max} = \max\{C_i, C_j\}$, the random and minimum assumptions give the total cloud cover as $C_{i,j}^{\text{ran}} = C_i + C_j - C_i \times C_j$ and $C_{i,j}^{\min} = \min\{C_i + C_j, 1\}$, respectively. Thus, the maximum assumption minimizes the total cloud cover, while minimum assumption produces minimally overlap between cloud layers and results in maximum total cloud cover (Weger et al., 1992). The total cloud cover predicted by the random assumption will fall somewhere between maximum and minimum assumption (Geleyn and Hollingsworth, 1979). For example, if the cloud covers in two model layers are 50%, then the maximum overlap will result in a total cloud cover of 50%, and a minimum overlap will result in an overcast condition (a complete cloud cover, i.e., 100%). These different overlap assumptions result in obvious different total cloud covers and will significantly affect the calculated radiative budgets and heating/cooling rate profiles (Morcrette and Fouquart, 1986; Barker et al., 1999; Barker and Fu, 2000; Chen et al., 2000; Pincus et al., 2005; Zhang et al., 2013a; 2013b; 2016; Jing et al.,

2016). Previously studies based on general circulation model (GCM) simulations indicated that the bias in the global mean radiation fluxes at the top of the atmosphere and at the surface can reach 20-40 W m⁻² due to the different overlap treatments (Morcrette and Jakob, 2000; Jing et al., 2009; Zhang and Jing, 2010).

Hogan and Illingworth (2000) revisited the cloud overlap assumptions and proposed a simpler and more useful expression for the degree of cloud layer overlap (exponential random overlap assumption) by using the ground-based radar measurement. In the expression, the observed cloud fraction of two cloud layers can be expressed as the linear combination of the maximum and random overlap by using a weighting factor, termed as cloud overlap parameter α :

$$\alpha = \frac{C_{i,j}^{obs} - C_{i,j}^{ran}}{C_{i,j}^{max} - C_{i,j}^{ran}} \quad (1)$$

The overlap parameter ranges from 0 (random) to 1 (maximum) when the observed total cloud cover falls between the values using the maximum and random overlap assumptions. The α will be negative when the degree of cloud overlap is lower than that predicted by the random overlap assumption. In the study of Hogan and Illingworth (2000), they also fitted the reduction in α with layer separation distance D as an inverse exponential function of the decorrelation length scale L : $\alpha = e^{-D/L}$.

Until now, many efforts that have been made to characterize the overlap parameter α and decorrelation length L using ground-based radar observations (e.g. Mace and Benson-Troth, 2002; Willén et al., 2005; Naud et al., 2008; Oreopoulos and Norris, 2011). For example, Oreopoulos and Norris (2011) derived L based on radar measurement taken over the US Southern Great Plains (SGP). Their results indicated that L ranges from 2 to 4.5 km across different seasons and smaller spatial scales correspond with smaller L values. Although radar can provide reliable cloud vertical structure profiles continuously, these observations are for a given location (Ge et al., 2017; 2018), and the radar sites are very sparsely distributed over the world, especially over the TP region where long-term Radar observations are nonexistent. Passive sensors and traditional surface weather reports fail to detect vertical cloud

structures, and only provide limited information about the cloud overlap (Chang and Li, 2005a, b; Huang, 2006; Huang et al., 2005, 2006a). The millimeter-wavelength cloud profiling radar (CPR) launched on CloudSat (Stephens et al., 2002) and the cloud-aerosol lidar with orthogonal polarization (CALIOP) (Winker et al., 2007) launched on CALIPSO (Cloud-Aerosol Lidar and Infrared Pathfinder Satellite Observation) provide an unprecedented opportunity to investigate vertical cloud overlaps on a global scale and to improve model representation of L (Barker et al., 2008; Kato et al., 2010; Mace et al., 2009; Li et al., 2011; 2015; Shonk et al. 2010; Shonk et al., 2014; Tompkins and Di Giuseppe, 2015; Di Giuseppe and Tompkins, 2015). Based on two months of cloud mask profile information from the CloudSat and CALIPSO satellites, Barker (2008) quantified the properties of cloud overlap on a global scale and found a wide range of L values, with a median value of 2 km. In other studies, L was usually a function of latitude or total cloud cover (Shonk et al., 2010; 2014; Yoo et al., 2014). Recently, Di Giuseppe and Tompkins (2015) further evaluated the impact of wind shear on the global-scale cloud overlap and identified an empirical relationship between the decorrelation length L and wind shear for use in models by using 6 months of CloudSat-CALIPSO data.

However, the related question of the cloud overlapping over the TP region has received little attention. It is still an open question on how the unique thermo-dynamic and dynamic environment over the TP region affects cloud overlap there. This study investigates the cloud overlap and its relation to the atmospheric states and large-scale atmospheric dynamics over the TP region by combining the cloud cover profile information from the 2B-GEOPROF-LIDAR dataset (Mace et al., 2009; Mace and Zhang, 2014) and the meteorological fields from the ERA-Interim reanalysis datasets (Dee et al., 2011). This paper is organized as follows. The datasets and methods used in this study are briefly described in Section 2. Section 3 outlines the monthly and zonal variations of the cloud overlap parameters over the TP region. The impacts of the atmospheric state and large-scale atmospheric dynamics on cloud overlap are presented in Sections 4. The conclusions and discussion are given in Section 5.

2. Datasets and methods

4 years (2007–2010) of data from the CloudSat 2B-GEOPROF-LIDAR, ECMWF-AUX and the daily 6-hour ERA-Interim reanalysis were used to analyze the impacts of atmospheric states and dynamics on the cloud overlap over the TP (27°N–39°N; 78°E–103°E) region (Fig. 1a).

2.1 Satellite datasets

Radar signals can penetrate the optically thick cloud layers that attenuate lidar signals, but lidar signals may sense the optically thin hydrometeor layers that are below the detection threshold of radar signals. Thus, with the unique complementary capabilities of the CPR on CloudSat and the CALIOP on the CALIPSO, the 2B-GEOPROF-LIDAR dataset produces the most accurate descriptions of the locations of the hydrometeor layers in the atmosphere on the global scale (Mace and Zhang, 2014). In this dataset, every CloudSat profile includes 125 height layers (e.g., vertical bin), and the “*CloudFraction*” parameter reports the fraction of the lidar volume within each radar vertical bin that contains hydrometeors (Mace et al., 2009; Mace and Zhang, 2014). Several previous studies have identified a cloudy atmospheric bin based on different thresholds of the lidar-identified cloud fraction, including a 99% (Barker, 2008; Di Giuseppe and Tompkins, 2015) or a 50% threshold (Haladay and Stephens, 2009; Verlinden et al., 2011). Here, a threshold of 99% is used in our study. Due to the significant attenuation of lidar signals to the optically thick layers, this parameter fails to provide the “*CloudFraction*” for optically thick layers. Thus, we also use the radar information (i.e., cloud “*LayerBase*” and “*LayerTop*” fields) from the aforementioned dataset to construct the complete two-dimensional cloud mask (See Fig. 1b). It is noting that the 2B-GEOPROF-LIDAR dataset does not distinguish cloud and precipitation, therefore any bias in our results caused by precipitation can't be removed in current analysis. Besides the 2B-GEOPROF-LIDAR dataset, the ECMWF-AUX dataset (Partain, 2004), which is an intermediate dataset that are the ancillary ECMWF state variables interpolated across each CloudSat CPR bin, are also used to provide the pressure and height information of each vertical bin in the cloud mask profile. The vertical and horizontal resolutions of these products are 240 m and 1.1 km, respectively. To avoid sunlight scattering contamination to lidar

observation and minimize surface contamination of the CPR, we only use the nighttime datasets above 1 km over the TP surface in our analysis.

210 2.2 Meteorological reanalysis dataset

The 6-hourly ERA-Interim reanalysis with a grid resolution of $0.25^\circ \times 0.25^\circ$ (Dee et al., 2011), is used to characterize the atmospheric thermodynamic and dynamic states over the TP. For each cloud mask profile in the 2B-GEOPROF-LIDAR, the vertical profiles of the zonal wind u , meridional wind v , relative humidity rh , specific
 215 humidity sh and atmospheric temperature T closest to the cloud profiles in both space and time are extracted and further interpolated vertically to match the vertical bins of the cloud mask profile. Following Di Giuseppe and Tompkins (2015), the u and v winds at every vertical bin are then projected onto the satellite overpass track, being averaged in the along-track direction for all profiles in the selected CloudSat data
 220 segment to derive the scene-average, along-track horizontal wind V . Here, we define the wind shear $dV/dz_{i,j}$ between the layers i and j , as follows:

$$dV/dz_{i,j} = \frac{\max\{V_i; V_j\} - \min\{V_i; V_j\}}{D_{i,j}}, \quad (2)$$

where V_i and V_j are the horizontal winds at layers i and j , respectively, and $D_{i,j}$ is the layer separation distance. The derived wind shear will be used to calculate the cloud
 225 overlap parameter. For the CloudSat overpass track (Fig. 1a), Di Giuseppe and Tompkins (2015) indicated that the cross-track shear of the zonal wind u has little statistical significance.

Similarly to the wind shear, we calculate the vertical gradient of the saturated equivalent potential temperature ($\partial\theta_{es}/\partial z_{i,j}$) between the same two layers to quantify
 230 the dependence of the cloud overlap on the degree of the conditional instability of the moist convection. Here,

$$\theta_{es} = \theta \exp\left(\frac{L_v r_s}{C_p T}\right)$$

$$\theta = T \left(\frac{1000}{p}\right)^{0.286}, L_v = 2.5 \times 10^6 - 2323 \times (T - 273.16) \quad (3)$$

$$r_{s=} = \frac{sh}{rh \times (1 - sh)}$$

where θ is the potential temperature, L_v is the latent heat of vaporization, r_s is the saturation mixing ratio, C_p is the specific heat capacity at a constant pressure, and T is the atmospheric temperature. The smaller the $\partial\theta_{es}/\partial z_{i,j}$, the more unstable the atmosphere. Furthermore, the scene-averaged vertical velocity at 500 hPa is extracted from the ERA-Interim reanalysis to analyze the impact of vertical motion on cloud overlap. The positive values are for the updraft, and negative values are for the subsidence.

2.3 The overlap parameter and dependence on the spatial scale

Previous studies have shown that the overlap parameter α and decorrelation length L are sensitive to the spatial scale of the GCM's grid box (Hogan and Illingworth, 2000; Oreopoulos and Khairoutdinov, 2003; Oreopoulos and Norris, 2011; Pincus et al., 2005). For example, Hogan and Illingworth (2000) found that cloud overlap parameter tends to increase with decreasing spatial and temporal resolution (i.e., increasing vertical and horizontal grid scales) of GCMs.

To examine the dependence of overlap parameter over TP on the spatial scale, each CloudSat orbit over the TP region is divided into segments with different horizontal lengths including 25, 50, 100 and 200 km. For convenience, this length is referred to as the spatial scale of the GCM's grid box. Fig.1b shows an example of cloud mask over the TP region from the 2B-GEOPROF-lidar dataset. This cloud mask includes eight, four, two and one segments, corresponding to the horizontal resolution of 25, 50, 100 and 200 km, respectively. Given the threshold of 99% for cloud fraction, the segment-average cloud cover profile of each segment is first derived. Here, it is important to emphasize that cloud fraction and cloud cover are different variables in our study. The “*Cloud fraction*” reports the fraction of lidar volumes in each radar vertical bin that contains hydrometeors and is used to identify a cloudy atmospheric

bin based on the chosen threshold, which is 99% in this paper. When averaging in the along-track direction for all cloud fraction profiles in a selected CloudSat data segment, we derive the segment-average cloud covers profile, which represents the percentage of clouds in a given spatial scale and certain height. Then, the vertical overlap between any two atmospheric layers in this profile is calculated when the cloud covers (C_i and C_j) of both layers exceed 0. Layers are analyzed in pairs and no ‘double-counting’. If two cloud layers have the same separation distance but different altitudes, they will be categorized into the same statistic group. Following Hogan and Illingworth (2000) and Di Giuseppe and Tompkins (2015), we consider the nonadjacent layers to be a continuous cloud pair when all layers between them are classified as cloud layers. Otherwise, these layers are classified as a non-continuous cloud pair (Hogan and Illingworth, 2000; Di Giuseppe and Tompkins, 2015).

Based on the definitions of different overlap assumptions and overlap parameter α in the introduction section, Figs.1c and 1d show an example of the observed and calculated segment-average cloud covers profile based on maximum and random assumptions, and corresponding cloud overlap parameter of continuous cloud pair for 25, 50, 100 and 200 km spatial scale in given cloud mask sample (Fig. 1b). It is clear that the observed and calculated cloud covers and corresponding overlap parameters tend to increase as the spatial scale increases. Meantime, the observed cloud covers tend to transform from the maximum to random overlap assumption with increasing layer separations.

By collecting 4 years of cloud sample from the 2B-GEOPROF-LIDAR dataset, Figs.2a and 2b further show the dependence of α on the layer separation and its sensitivity to the spatial scale for both non-continuous and continuous cloud pairs. Many studies have used ground- and space-based radar to examine the validity of the random overlap assumption for the vertically non-continuous clouds (Hogan and Illingworth, 2000; Mace et al., 2002; Naud et al., 2008; Di Giuseppe and Tompkins, 2015). Fig.2a shows that the degree of cloud overlap of the non-continuous clouds over the TP region is lower than the random overlap, especially when the layer separation is smaller than 2km. Given the spatial scale of 50 km, almost all the α

-values are negative and fall between -0.25 and -0.05. Thus, the total cloud cover would still slightly be underestimated for non-continuous cloud pairs by using the random overlap assumption. Assuming a cloud layer separation of less than 9 km, α for non-continuous cloud pairs increases as the spatial scale increases (e.g., from 25 km to 200 km). For a continuous cloud pair (Fig. 2b), α decrease from 0.95 to 0 with an increasing separation. Meantime, a slight dependence of α on the spatial scale is also observed for continuous cloud pairs when they are separated by a distance of about 1 km to 4 km. This indicates that a maximum overlap is slightly more common for a larger horizontal domain, which is consistent with previous studies (Hogan and Illingworth, 2000; Oreopoulos and Khairoutdinov, 2003; Oreopoulos and Norris, 2011).

2.4 Selection of thresholds for cloud cover and spatial scale

About the dependence of α on the spatial scale, Tompkins and Di Giuseppe (2015) theorized that some overcast or single cloud layers would be removed from the samples when the spatial scale is smaller than the cloud system scale, thus biasing α and its decorrelation length. Given a spatial scale of 50 km, the ratio of the spatial scale to the cloud system scale decreases strongly from the equator to the poles because many of the frontal cloud systems of the middle and high latitudes are larger than the convective cloud systems over the tropics. Ultimately, the corresponding bias of α would increase with latitude. Thus, regional atmospheric models should account for the typical cloud system scales in their parameterization schemes when using a fixed horizontal resolution.

Fig. 2c depicts the probability distribution functions (PDFs) of the horizontal scales of the along-track cloud systems at different heights over the TP region. Here, the horizontal scale of a cloud system at a given height along the CALIPSO/CloudSat track is determined by calculating the number of continuous cloud profiles (N) at a given height. Using a 1.1 km along-track resolution for the CPR measurements, the along-track scale (S) of a cloud system is $S=N \times 1.1$ km (Zhang et al., 2014; Li et al., 2015). It is clear that the probability of a small-scale cloud system decreases with an increasing height (Fig.2c). The mean horizontal scale of 59.2 km for a cloud system at

a height of 15 km is almost twelve times greater than that (i.e., 4.6 km) at a height of 2 km. For TP region, we can see that the horizontal scales of cloud system below 10 km are smaller than the spatial scale of 50 km, thus we apply the spatial scale of 50 km to perform the following analysis although this scale would still result in significant errors in α at higher atmospheric heights (e.g., 15km) where cloud has large horizontal scale.

In addition, to further reduce the sensitivity of α to the spatial scale caused by data truncation, we also apply a simple data filter following Tompkins and Di Giuseppe (2015) so that only atmospheric layers with segment-average cloud covers smaller than a given threshold of 50% are retained. As stated by Tompkins and Di Giuseppe (2015), data might still be truncated with this filter, but the sensitivity of the results to the spatial scale should largely be reduced. By limiting the spatial scale (50 km) and upper limit of cloud cover (50%), the number of available cloud layer-pair samples is still at least one million, thus ensuring statistical significance. Fig. 2d shows the variations of cloud sample numbers and the cumulative percentages with cloud layer separations for both non-continuous and continuous clouds at a given spatial scale of 50km. It shows that the cumulative proportion of cloud samples significantly increases with layer separation. For the continuous cloud, the cumulative percentage accounts for 90% of all samples when layer separation is smaller than 4 km. Given the 1.1 km along-track resolution of the CPR measurements and a spatial scale of 50 km (that is, about 50 CloudSat profiles), the each cloudy CloudSat profile has a cloud cover about 2% (Di Giuseppe and Tompkins, 2015).

3. Monthly and zonal variations of overlap parameter for continuous clouds

Figure 3a shows the monthly variations in α for the continuous cloud-pair based on pentad-average over the TP. In Fig.3a, the maximum continuous cloud layer separation gradually increases from January (approximately 6 km) to August (beyond 8 km) and then gradually decreases, indicating that cloud systems over TP during summer are thicker than other seasons due to frequent strong convective motions. When the cloud layer separation is less than 1 km, the overlap parameter α has little monthly variation and is always large (even beyond 0.7). However, the monthly

variation of α becomes manifest with a layer separation larger than 1 km. For a 2-km cloud separation, e.g., α reaches its maximum of 0.45 in August and a minimum of 0.1 in February (see Fig. 3d). For a separation of 3 km, α is generally lower but has the similar monthly variation to those seen for a 2-km separation. By checking the negative value of α in Fig.3a, it is clear that even random overlap assumption could underestimate the total cloud cover between two cloud layers with large separation during all seasons except summer. These cloud overlap features may be associated with the unique topographical forcing and corresponding thermo-dynamic and dynamic environment of the TP. In summer, the TP is usually considered as an atmospheric heat source or “air pump” due to its higher surface temperature compared with surrounding regions at the same altitude (Wu et al., 2015). Additionally, a humid and warm air intrudes from the South Asia monsoon area into the lower atmosphere over the TP would intensify the atmospheric instability of moist convection when combined with the enhanced surface heating (Taniguchi and Koike, 2008). This process further promotes the transportation of water vapor into high altitudes and favors the development of convective clouds. Indeed, satellite observations have indicated that cumulus prevails over the TP during the summer (Wang et al., 2014; Li and Zhang, 2016).

Noting a small horizontal scale of cumulus, a 50 km-spatial scale from CloudSat should not bias α estimate too much in our study. However, previous studies have pointed out that precipitation may bias the cloud overlap statistics toward maximum overlap (Mace et al., 2009; Di Giuseppe and Tompkins, 2015). Present studies did not eliminate the influence of precipitation on the overlap parameter. The overlap parameter α would become smaller if the samples with precipitation are removed from the analysis. The feature may be even more obvious during summer due to more frequent precipitation over TP during this season (Yan et al., 2016). The seasonal variation of α was also found at different ground sites (Mace and Benson-Troth, 2002; Naud et al., 2008). For example, Oreopoulos and Norris (2011) indicated that clouds tend to be more random in the winter and most maximum during the summer. In fact, these overlap properties are associated with cloud system scale, which is

dominated by dynamical situation (Tompkins and Di Giuseppe, 2015).

Figures 3b and 3c show the monthly variations in pentad-averaged conditional
380 instability of the moisture convection ($\partial\theta_{es}/\partial z$) and the wind shear (dV/dz) for the
continuous cloud-pairs over the TP, respectively. The $\partial\theta_{es}/\partial z$ and dV/dz both
exhibit obvious monthly variations for all cloud-layer separations. The atmospheric
stability and wind shear gradually decrease from January to August and then steadily
increase (see Figs. 3c, 3d, 3e and 3f). From Fig.3c, we see that adjacent atmospheric
385 layers during May to September tend to be more unstable and have weak wind shear.
These atmospheric states favor the development of clouds and result in maximum
overlap between cloud layers. During other month (e.g., December), clouds also tend
to follow the maximum overlap more although adjacent atmospheric layers are stable
with large $\partial\theta_{es}/\partial z$ and dV/dz . It might be the case that vertical velocities might be
390 large because of extratropical cyclones or other baroclinic instability. With the layer
separation increases, atmospheric layers become more stable and then favor random
overlap, especially during summer season. These results verify that a more unstable
atmosphere tends to favor a maximum overlap over a random one, as shown in
previous studies (Mace and Benson-Troth, 2002; Naud et al., 2008). Note that Figs. 3d
395 and 3f might reveal an inconsistency between the wind shear and atmospheric stability.
For example, we can see that the wind shear for a 2-km layer distance is greater than
that for a 3-km distance, but the atmosphere is also more unstable. This inconsistency
is probably because two cloud layers with the same separation but at different
altitudes are sorted into the same statistical group. Or, it is also quite possible that
400 other large scale forcings might influence the overlap. In addition, we find the
monthly variations in pentad-averaged vertical velocity (ω) at 500 hPa (see Figs.3g
and 3h) are also consistent with the monthly cycle of α . It means that vigorous ascent
tends to favor maximum overlap. This result agrees well with the previous studies
(Naud et al., 2008).

405 Figure 4 shows the zonal variations of α , $\partial\theta_{es}/\partial z$, dV/dz and ω over the TP.

Figs. 4a and 4b indicate that α is larger in the south part of the TP and smaller to the north. This is mainly because the atmospheric instability over the southern part of the TP enhances the convective activity (Fujinami and Yasunari, 2001). Due to the weakening of the monsoon and the blocking by topography, less water vapor may reach the northern part, and thus fewer clouds from there (You et al., 2014). Compared with the southern TP, the stability and wind shear are both larger over the northern part, especially for those cloud layers with large separation (e.g., >2km). This meteorological condition will result in more frequent negative α , indicating that random overlap assumption used in models would underestimate the total cloud cover and thus bias the surface radiation over these regions (see Fig.4a). The most significant warming occurring over the Northern part of TP has been attributed to pronounced stratospheric ozone depletion (e.g., Guo and Wang, 2012). However, a more recent study indicates that the accelerated warming trend over the Tibetan Plateau may be due to the rapid cloud cover increases at nighttime over the northern Tibetan Plateau and the sunshine duration increase in the daytime over the southern Tibetan Plateau (Duan and Xiao, 2015). Therefore an accurate representation of total cloud cover and its relations to atmospheric thermodynamic and dynamic conditions in models is critically important to the understanding of the TP rapid warming. Although it is still difficult for models to capture the cloud overlap properties, especially for those cloud layers with large separation over north TP, our results confirm that α is well related with wind shear and instability. However, the zonal variation of α is inconsistent with the variation of vertical velocity (see Figs. 4g and 4h).

4. Sensitivity of α on the meteorological conditions and its parameterization

To facilitate the parameterization of α for cases of continuous clouds, we further investigate the sensitivity of α on the different meteorological conditions. Here, each meteorological factor over the TP region is grouped into one of four bins as follows. The four bins for $\partial\theta_{es}/\partial z$ are $\partial\theta_{es}/\partial z > 5$ K/km, $2.5 < \partial\theta_{es}/\partial z < 5$ K/km, $0 < \partial\theta_{es}/\partial z < 2.5$ K/km and $\partial\theta_{es}/\partial z < 0$ K/km. For wind shear, the four bins

435 are $dV/dz < 0.5 \text{ m} \cdot \text{s}^{-1}/\text{km}$, $0.5 < dV/dz < 2 \text{ m} \cdot \text{s}^{-1}/\text{km}$, $2 < dV/dz < 3.5 \text{ m} \cdot \text{s}^{-1}/\text{km}$
and $dV/dz > 3.5 \text{ m} \cdot \text{s}^{-1}/\text{km}$. For vertical velocity, the four bins are $\omega < -40 \text{ hPa/day}$,
 $-40 < \omega < 0 \text{ hPa/day}$, $0 < \omega < 40 \text{ hPa/day}$ and $\omega > 40 \text{ hPa/day}$. These groupings
ensure that a statistically significant number of samples fall within each bin (i.e., at
least one hundred thousand samples per bin). In addition, Li et al. (2015) indicated
440 that the overlap properties between different cloud types are obvious different but the
most significant components of the global climate system. Although current study
doesn't include the information of cloud type, the sensitivity of α on the
meteorological parameters in our analysis actually exhibit the effects of cloud types
due to different cloud types with same layer separation possibly take place in distinct
445 wind shear and stability conditions.

Figure 5 illustrates the sensitivity of α to wind shear, instability and vertical
velocity at given upper limit of cloud cover (50%) and spatial scale (50 km) for the
continuous clouds. Since the cloud samples with layer separations smaller than 3.5 km
account for 90% of all samples for continuous clouds, we only present the results for
450 layer distances smaller than 3.5 km. Naud et al. (2008) tested the sensitivity of α to
wind shear at three sites and found that wind shear slightly affects α when the layer
distance is larger than 2 km. In a recent study, Di Giuseppe and Tompkins (2015)
demonstrated the important effect of wind shear on the global cloud overlap by using
a combination of the CloudSat-CALIPSO cloud data and the ECMWF reanalysis
455 dataset. Our results along with previous studies suggest that the cloud overlap strongly
depends on atmospheric conditions, but their relationship displays some variability, in
particular spatially and seasonally. The effect of the atmospheric stability on cloud
overlap may be more important over convective regions (e.g., the intertropical
convergence zone and TP during summer season) while the effect of wind shear may
460 be dominant over the mid-latitudes. Besides the wind shear and instability, some
studies also tested the sensitivity of the overlap parameter to the large-scale vertical
velocity. For example, Naud et al. (2008) indicated that vertical velocities in the
tropics are not captured in the reanalysis dataset when convection occurs, thus they

only discussed the impact of vertical velocity on the cloud overlap parameter over the
 465 mid-latitude and found that vigorous ascent tends to favor maximum overlap. Fig.5c
 shows that vertical velocity at 500hPa has an effect to cloud overlap parameter.
 However, by combining the effects of wind shear, instability and vertical velocity in
 parameterizations of decorrelation length scale L , we find that this scheme doesn't
 show better superiority than the scheme which only includes the wind shear and
 470 instability. Thus, we only parameterize decorrelation length scale L as a function of
 the wind shear and atmospheric stability in current study.

Here, we derive the decorrelation length scale L values (km) from the least
 squares exponential fit to the original α curve at given wind shear and instability
 bin. We parameterize L as a function of wind shear or both wind shear and
 475 atmospheric instability based on a (multiple) linear regression. The regression formula
 of L can be written as:

$$L = L_{\alpha} - b1 \frac{\partial \theta_{es}}{dz} - b2 \frac{dV}{dz}$$

or

$$L = L_{\alpha1} - c1 \frac{dV}{dz}$$
(4)

Here, L_{α} , $L_{\alpha1}$, $b1$, $b2$, and $c1$ are the fitting parameters. Table 1 lists several
 parameterization schemes for the decorrelation length scale L . The scheme with wind
 480 shear from Di Giuseppe and Tompkins (2015) using the global CloudSat-CALIPSO
 cloud data and ECMWF reanalysis dataset is shown for a comparison. Di Giuseppe
 and Tompkins (2015) discussed the uncertainties from fitting methods and calculation
 of wind shear. Related to the observational orbit, the impact of cross-track wind shear
 is neglected in our study, which would exclude many large wind shear associated with
 485 jet structures (Di Giuseppe and Tompkins, 2015). The parameterization scheme of
 Shonk et al. (2010) is also shown in Table 1, which is an empirical linear relationship
 between L and latitude based on CloudSat and CALIPSO data. Our parameterization
 schemes in terms of wind shear or both wind shear and instability are given in Table 1.
 Note that the R-squared values (R^2) for our wind shear and wind shear-instability

490 schemes are 0.88 and 0.96, respectively.

After deriving the regression formula of decorrelation length scale L , we re-apply it to all continuous cloud samples and retrieve the L and corresponding α based on the formula: $\alpha = e^{-D/L}$ and cloud layer separation. Finally, retrieved overlap parameter α is used to calculate the cloud cover between any two cloud layers by using the Equ.(1) and definitions of random and maximum overlap assumptions. Figure 6 presents the monthly difference between calculated and observed cloud covers using various overlap parameterization schemes. It is seen that the maximum and random overlap assumptions result in large cloud cover biases, especially for layer separations greater than 1 km for maximum overlap and less than 2 km for random overlap where the bias exceeds 5%. Compared with random and maximum assumptions, the differences of cloud over caused by other schemes are small and range from -3% to 3%. In addition the wind shear scheme and the wind shear-instability scheme from the present studies overall show less biases than other schemes. However, several points still need further attention. First, the wind shear scheme from Di Giuseppe and Tompkins (2015) significantly underestimates the cloud cover for layer separations above 1 km (e.g., reach 3%). This large bias may be because it is based on the global CloudSat-CALIPSO measurements and ECMWF reanalysis dataset for a short period (January-July 2008); as such, some obvious regional or seasonal cloud overlap properties are easily obscured by global averaging. Furthermore the role of atmospheric stability was not considered in this scheme. However, the scheme from Di Giuseppe and Tompkins (2015) causes little bias for layer separations below 1 km. This is because this scheme retrieves much larger L and overlap parameter values than other schemes. An interesting finding is that Shonk/latitude scheme leads to comparable bias with new schemes from this study. The bias is even smaller for Shonk/latitude scheme when the layer separation is below 1 km. In fact, Fig.5 has demonstrated that the sensitivity of α to wind shear and instability is rather weak when cloud layers are very close. Compared with our wind shear scheme, our wind shear-instability scheme further combines the impact of atmospheric instability and

has a relatively lower bias at large layer separations with higher R-squared values
($R^2=0.96$).

Fig.7 shows the zonal difference between calculated and observed cloud covers for the aforementioned schemes. The differences of cloud cover caused by different overlap schemes are distinguishable. Similar with Fig.6, the maximum and random overlap assumptions still result in the most prominent cloud cover biases (exceed \pm 5%) at most of the layer separations. Compared with our wind shear scheme and wind shear-instability schemes, the scheme from Di Giuseppe and Tompkins (2015) and latitude scheme from Shonk et al. (2010) cause relatively obvious underestimation of total cloud cover when cloud layer separations exceed 1 km, especially for scheme from Di Giuseppe and Tompkins (2015) (bias reach -3%). Only if cloud layer separations are smaller than 1 km, these two schemes produce better cloud cover simulation than our schemes. In summary, these results indicate that new parameterization (that is, our wind shear-instability scheme) of decorrelation length scale, which includes the effects of both wind shear and atmospheric stability on cloud overlap, may improve the prediction of cloud cover over TP.

5. Conclusions and discussion

The Tibetan Plateau has experienced a rapid warming over the past three decades. Previous studies suggests that the change in cloud cover may explain different temperature trends in the daytime and nighttime over the TP (Duan and Wu, 2006; Kang et al., 2010). Indeed, many studies have verified that annual and seasonal total cloud amounts have declined over TP (e.g., Yang et al., 2012; You et al., 2014), leading to the increase of absorbed solar radiation and the increase of surface air temperatures (Duan and Xiao, 2015).

To accurately simulate the total cloud cover and its impact on the radiative energy budget, climate models need to reliably represent the cloud vertical overlap, which has received less attention than necessary because of the limited regional cloud observations. In this study, we analyze 4 years (2007–2010) of data over the Tibetan Plateau from the CloudSat 2B-GEOPROF-LIDAR dataset and the ECMWF-AUX dataset and along with the ERA-Interim daily 6-hourly reanalysis. It is confirmed that

the continuous cloud layers tend to have maximum overlap at small separation but
 550 gradually become randomly overlapped with an increase of the layer separation.
 Focusing on the continuous cloud layers, we evaluate the effects of the meteorological
 conditions on the cloud overlap. It is found that the unstable atmospheric stratification
 with a weak wind shear over the TP would tend to favor maximum overlap (that is,
 greater α values), agreeing well with previous studies. We parameterize the
 555 decorrelation length scale L , a parameter that is used to characterize the transition
 from the maximum to random overlap assumption, as a function of the wind shear and
 atmospheric stability. Compared with other parameterizations, this new scheme
 improves the prediction of cloud cover over TP when cloud layers separations are
 greater than 1km. Although the parameterization method derived in our study focuses
 560 only on the TP, our results suggest that the parameterization of the decorrelation
 length scale L by considering multiple thermodynamic and dynamic factors and
 microphysical effects (e.g., precipitation) has the potential to improve the
 model-simulated total cloud covers.

In a recent study, Di Giuseppe and Tompkins (2015) applied the wind
 565 shear-dependent decorrelation length scale in the ECMWF Integrated Forecasting
 System. They found that the impact of wind shear-dependent parameterization on
 radiative budget calculation is comparable in magnitude to that of latitude-dependent
 scheme of Shonk et al. (2010). Our results also show that latitude-dependent scheme
 has similar bias of cloud cover relative to the new scheme developed in this study.
 570 Although these results can't suggest which of the scheme is superior, the scheme
 based on factor the meteorological factors has some potential advantages. For
 example, cloud overlap parameter is significantly controlled by atmospheric
 thermodynamic and dynamic conditions, therefore the long-term variations of
 meteorological factors are bound to affect the trend of cloud overlap and the resulting
 575 in total cloud cover and radiation budget. Indeed, a recent study has shown that rapid
 warming and an increase of atmospheric instability over the TP leads to more frequent
 deep clouds, which are responsible for the reduction of solar radiation over the TP
 (Yang et al., 2012). By using surface observations over 71 stations, some studies

verified that annual and seasonal total cloud covers have declined during 1961-2005
 580 (Duan and Wu, 2006; You et al., 2014). However, whether such variations of total
 cloud cover are linked with the changes of degree of cloud overlap over the TP are
 still unclear. Thus, more efforts are needed to reasonably evaluate the impact of cloud
 overlap on the total cloud cover variations over these sensitive areas of climatic
 change (e.g., Tibetan Plateau and Arctic).

585 ***Competing interests.*** The authors declare that they have no conflict of interest.

Acknowledgements. This research was jointly supported by the key Program of the
 National Natural Science Foundation of China (41430425), the Foundation for
 590 Innovative Research Groups of the National Science Foundation of China (grant no.
 41521004), National Science Foundation of China (grant nos. 41575015 and
 41575143) and the China 111 project (grant no. B13045). We would like to thank the
 CALIPSO, CloudSat and ERA-Interim science teams for providing excellent and
 accessible data products that made this study possible. The CloudSat datasets are
 595 available from this link: (<http://www.cloudsat.cira.colostate.edu/order-data>), and
 ERA-Interim daily product may be accessed from
 (<http://apps.ecmwf.int/datasets/data/interim-full-daily/levtype=pl/>).

References

- 600 Barker, H. W., Stephens, G. L., and Fu, Q.: The sensitivity of domain-averaged solar fluxes to
 assumptions about cloud geometry, *Quart. J. R. Meteorol. Soc.*, 125, 2127-2152, 1999.
 Barker, H.W., and Fu, Q.: Assessment and optimization of the Gamma-weighted two-stream
 approximation, *J. Atmos. Sci.*, 57, 1181-1188, 2000.
 Barker, H. W.: Overlap of fractional cloud for radiation calculations in GCMs: A global analysis
 605 using CloudSat and CALIPSO data, *J. Geophys. Res.*, 113(113), 762-770, 2008.
 Boucher, O., Randall, D., Artaxo, P., Bretherton, C., Feingold, G., Forster, P., Kerminen, V.-M.,
 Kondo, Y., Liao, H., Lohmann, U., Rasch, P., Satheesh, S. K., Sherwood, S., Stevens, B., and
 Zhang, X. Y.: Clouds and aerosols, in: *Climate Change 2013: The Physical Science Basis*.
 Contribution of Working Group I to the Fifth Assessment Report of the Intergovernmental
 610 Panel on Climate Change, edited by: Stocker, T. F., Qin, D., Plattner, G.-K., Tignor, M.,
 Allen, S. K., Doschung, J., Nauels, A., Xia, Y., Bex, V., and Midgley, P. M.: Cambridge

University Press, United Kingdom and New York USA, 571–657,
doi:10.1017/CBO9781107415324.016, 2013.

- 615 Chang, F. L., and Li, Z.: A New Method for Detection of Cirrus Overlapping Water Clouds and
Determination of Their Optical Properties, *J. Atmos. Sci.*, 62(11), 3993–4009, 2005a.
- Chang, F. L., and Li, Z.: A near global climatology of single-layer and overlapped clouds and their
optical properties retrieved from TERRA/MODIS data using a new algorithm, *J. Clim.*, 18,
4752–4771, 2005b.
- 620 Chen, B., and Liu, X.: Seasonal migration of cirrus clouds over the Asian Monsoon regions and
the Tibetan Plateau measured from MODIS/Terra, *Geophys. Res. Lett.*, 32(320), 67–106,
2005.
- Chen, T., Rossow, W. B., and Zhang, Y.: Radiative Effects of Cloud-Type Variations, *J. Clim.*, 13,
264–286, 2000.
- 625 Cheng, G. and Wu, T.: Responses of permafrost to climate change and their environmental
significance, Qinghai – Tibet Plateau, *J. Geophys. Res.*, 112 (F2), F02S03, 2007.
- Dee, D. P., Uppala, S. M., Simmons, A. J., Berrisford, P., Poli, P., Kobayashi, S., Andrae, U.,
Balmaseda, M., A. Balsamo, G., Bauer, P., Bechtold, P., Beljaars, A. C. M., Van De Berg, L.,
Bidlot, J., Bormann, N., Delsol, C., Dragani, R., Fuentes, M., Geer, A., J. Haimberger, L.,
Healy, S. B., Hersbach, H., Hõm, E. V., Isaksen, L., Kållberg, P., Köhler, M., Matricardi, M.,
630 McNally, A. P., Monge-Sanz, B. M., Morcrette, J. J., Park, B. K., Peubey, C., De Rosnay, P.,
Tavolato, C., Thépaut, J. N., and Vitart, F.: The ERA-Interim reanalysis: configuration and
performance of the data assimilation system, *Quart. J. R. Meteorol. Soc.*, 137(656), 553–597,
2011.
- Di Giuseppe, F., and Tompkins, A. M.: Generalizing Cloud Overlap Treatment to Include the
635 Effect of Wind Shear, *J. Atmos. Sci.*, 72, 2865–2876, 2015.
- Duan, A., and Xiao, Z.: Does the climate warming hiatus exist over the Tibetan Plateau?,
Scientific Reports, 5, 13711, 2015.
- Duan, A., Wang, M., Lei, Y. and Cui, Y.: Trends in summer rainfall over China associated with
the Tibetan Plateau sensible heat source during 1980 – 2008, *J. Clim.*, 26, 261 – 275, 2013.
- 640 Duan, A., and Wu, G.: Change of cloud amount and the climate warming on the Tibetan Plateau,
Geophys. Res. Lett., 33(22), 395–403, 2006.
- Duan, A. M., and Wu, G. X.: Role of the Tibetan Plateau thermal forcing in the summer climate
patterns over subtropical Asia, *Clim. Dyn.*, 24(7), 793–807, 2005.
- 645 Fu, Q., and Liou, K. N.: Parameterization of the radiative properties of cirrus clouds, *J. Atmos.*
Sci., 50, 2008–2025, 1993.
- Fu, Q., Cribb, M.C., Barker, H.W., Krueger, S.K., and Grossman, A. 2000: Cloud geometry
effects on atmospheric solar absorption, *J. Atmos. Sci.*, 57, 1156–1168, 2000;
- Fu, Q., Baker, M., and Hartmann, D. L.: Tropical cirrus and water vapor: An effective earth
infrared iris feedback? *Atmos. Chem. Phys.*, 2, 1–7, 2002.
- 650 Fujinami, H., and Yasunari, T.: The seasonal and intraseasonal variability of diurnal cloud activity
over the Tibetan Plateau, *J. Meteor. Soc. Japan*, 79, 1207–1227, 2001.
- Ge, J., Zhu, Z., Zheng, C., Xie, H., Zhou, T., Huang, J., and Fu, Q.: An improved hydrometeor
detection method for millimeter-wavelength cloud radar, *Atmos. Chem. Phys.*, 17, 9035–9047,
<https://doi.org/10.5194/acp-17-9035-2017>, 2017.

- 655 Ge, J., Zheng C., Xie H., Xin Y., Huang J., and Fu Q.: Mid-latitude Cirrus Cloud at the SACOL site: Macrophysical Properties and Large-Scale Atmospheric State, *J. Geophys. Res.*, doi: 10.1002/2017JD027724, 2018
- Geleyn, J. F., and Hollingsworth, A.: An economical analytical method for the computation of the interaction between scattering and line absorption of radiation, *Contrib. Atmos. Phys.*, 52, 1–16, 1979.
- 660 Guo, D., and Wang, H.: The significant climate warming in the northern Tibetan Plateau and its possible causes, *Int. J. Climatol.* 32, 1775 – 1781. <http://dx.doi.org/10.1002/joc.2388>, 2012.
- Haladay, T., and Stephens, G.: Characteristics of tropical thin cirrus clouds deduced from joint CloudSat and CALIPSO observations, *J. Geophys. Res.*, 114(114), D00A25-D00A37, 2009.
- 665 Hartmann, D. L., Ockert-Bell, M. E., and Michelsen, M. L.: The effect of cloud type on Earth's energy balance: Global analysis, *J. Clim.*, 5(11), 1281-1304, 1992.
- Hogan, R. J., and Illingworth, A. J.: Deriving cloud overlap statistics from radar, *Quart. J. R. Meteorol. Soc.*, 126(569), 2903-2909, 2000.
- Huang, J. P., Minnis, P., and Lin, B.: Determination of ice water path in ice- over-water cloud systems using combined MODIS and AMSR-E measurements, *Geophys. Res. Lett.*, 33, L21801, doi: 10.1029/2006GL027038, 2006a.
- 670 Huang, J. P.: Analysis of ice water path retrieval errors over tropical ocean, *Adv. Atmos. Sci.*, 23, 165–180, 2006b.
- Huang, J. P., Minnis, P., and Lin, B.: Advanced retrievals of multilayered cloud properties using multispectral measurements, *J. Geophys. Res.*, 110, D15S18, doi: 10.1029/2004JD005101, 2005.
- 675 Jing, X., Zhang, H., Peng, J., Li, J., and Barker, H. W.: Cloud overlapping parameter obtained from CloudSat/CALIPSO dataset and its application in AGCM with McICA scheme, *Atmos. Res.*, 170, 52-65, 2016.
- 680 Jing, X., Zhang H., and Guo P.: A study of the effect of sub-grid cloud structure on global radiation in climate models, *Acta. Meteor. Sinica*, 67, 1058-1068, 2009.
- Kang, S., Xu, Y., You, Q., Flügel, W.A., Pepin, N. and Yao, T.: Review of climate and cryospheric change in the Tibetan Plateau, *Environ. Res. Lett.*, 5, 015101. <http://dx.doi.org/10.1088/1748-9326/5/1/015101>, 2010.
- 685 Kato, S., Sun-Mack, S., Miller, W. F., Rose, F. G., Chen, Y., Minnis, P., and Wielicki, B. A.: Relationships among cloud occurrence frequency, overlap, and effective thickness derived from CALIPSO and CloudSat merged cloud vertical profiles, *J. Geophys. Res.*, 115(D4), 1-28, 2010.
- Kawamoto, K. and Suzuki, K.: Microphysical transition in water clouds Over the Amazon and China derived from spaceborne radar and Radiometer data, *J. Geophys. Res.*, 117, D05212, doi: 10.1029/2011JD016412, 2012.
- 690 Li, J., Huang, J., Stamnes, K., Wang, T., Lv, Q., and Jin, H.: A global survey of cloud overlap based on CALIPSO and CloudSat measurements, *Atmos. Chem. Phys.*, 15(1), 519-536, 2015.
- 695 Li, J., Hu, Y., Huang, J., Stamnes, K., Yi, Y., and Stamnes, S.: A new method for retrieval of the extinction coefficient of water clouds by using the tail of the CALIOP signal, *Atmos. Chem. Phys.*, 11(6), 2903-2916, 2011.

Li, J., Yi, Y., Minnis, P., Huang, J., Yan, H., Ma, Y., Wang, W., and Ayers, K.: Radiative effect differences between multi-layered and single-layer clouds derived from CERES, CALIPSO, and CloudSat data, *J. Quant. Spectrosc. Radiat. Transf.*, 112, 361-375, 2011.

Li, Y., Liu, X., and Chen B.: Cloud type climatology over the Tibetan Plateau: A comparison of ISCCP and MODIS/TERRA measurements with surface observations, *Geophys. Res. Lett.*, 33, L17716, doi: 10.1029/2006GL026890, 2006.

Li, Y. Y., and Zhang, M.: Cumulus over the Tibetan Plateau in the summer based on CloudSat–CALIPSO data, *J. Climate*, 29, 1219–1230, doi:10.1175/JCLI-D-15-0492.1, 2016.

Mace, G. G., and Zhang, Q.: The CloudSat radar-lidar geometrical profile product (RL-GeoProf): Updates, improvements, and selected results, *J. Geophys. Res.*, 119(15), 9441-9462, doi: 10.1002/2013JD021374, 2014.

Mace, G. G., Zhang, Q., Vaughan, M., Marchand, R., Stephens, G., Trepte, C., and Winker, D.: A description of hydrometeor layer occurrence statistics derived from the first year of merged CloudSat and CALIPSO data, *J. Geophys. Res.*, 114, D00A26, doi: 10.1029/2007JD009755, 2009.

Mace, G. G., and Bensonroth, S.: Cloud-Layer Overlap Characteristics Derived from Long-Term Cloud Radar Data, *J. Clim.*, 15(17), 2505-2515, 2002.

Morcrette, J. J., and Jakob, C.: The response of the ECMWF model to changes in the cloud overlap assumption, *Mon. Wea. Rev.*, 128, 1707–1732, 2000.

Morcrette, J. J., and Fouquart, Y.: The Overlapping of Cloud Layers in Shortwave Radiation Parameterizations, *J. Atmos. Sci.*, 43(4), 321-328, 1986.

Naud, C. M., Del Genio, A., Mace, G. G., Benson, S., Clothiaux, E. E., and Kollias, P.: Impact of dynamics and atmospheric state on cloud vertical overlap, *J. Clim.*, 21(8), 1758-1770, 2008.

Oreopoulos, L., and Norris, P. M.: An analysis of cloud overlap at a midlatitude atmospheric observation facility, *Atmos. Chem. Phys.*, 11(1), 5557-5567, 2011.

Oreopoulos, L., and Khairoutdinov, M.: Overlap properties of clouds generated by a cloud-resolving model, *J. Geophys. Res.*, 108, 4479, doi: 10.1029/2002JD003329, 2003.

Pincus, R., Hannay, C., Klein, S. A., Xu, K. M., and Hemler, R.: Overlap assumptions for assumed probability distribution function cloud schemes in large-scale models, *J. Geophys. Res.*, 110(D15), 2005.

Rossow, W. B., Gardner, L. C., and Lacis, A. A.: Global seasonal cloud variations from satellite radiance measurements. Part I: sensitivity of analysis, *J. Clim.*, 2, 419-458, 1989.

Shonk, J. K. P., Hogan, R. J., and Manners, J.: Impact of improved representation of horizontal and vertical cloud structure in a climate model, *Clim. Dyn.*, 38, 2365-2376, 2014.

Shonk, J. K., Hogan, R. J., Edwards, J. M., and Mace, G. G.: Effect of improving representation of horizontal and vertical cloud structure on the Earth's global radiation budget. Part I: Review and parametrization, *Quart. J. R. Meteorol. Soc.*, 136(650), 1191-1204, 2010.

Stephens, G. L.: Cloud feedbacks in the climate system: a critical review, *J. Clim.*, 18, 237-273, 2005.

Stephens, G. L., Vane, D. G., Boain, R. J., Mace, G. G., Sassen, K., Wang, Z., Illingworth, A. J., O'Connor, E. J., Rossow, W. B., Durden, S. L., Miller, S. D., Austin, R. T., Benedetti, A., Mitrescu, C., and CloudSat Science Team.: The CloudSat mission and the A-Train, A new dimension of space-based observations of clouds and precipitation, *B. Am. Meteor. Soc.*, 83,

1771-1790, 2002.

Taniguchi, K., and Koike, T.: Seasonal variation of cloud activity and atmospheric profiles over the eastern part of the Tibetan Plateau. *J. Geophys. Res.*, 113(D10), 523-531, 2008.

745 Tompkins, A., and Giuseppe, F. D.: An interpretation of cloud overlap statistics, *J. Atmos. Sci.*, 72, 2877-2889, 2015.

Verlinden, K. L., Thompson, D. W. J., and Stephens, G. L.: The Three-Dimensional Distribution of Clouds over the Southern Hemisphere High Latitudes, *J. Clim.*, 24(24), 5799-5811, 2011.

Wang, B., Bao, Q., Hoskins, B., Wu, G. and Liu, Y.: Tibetan Plateau warming and precipitation changes in East Asia, *Geophys. Res. Lett.*, 35, L14702, 2008

750 Wang, M. Y., Gu, J., Yang, R., Zeng, L. and Wang, S.: Comparison of cloud type and frequency over China from surface, FY-2E, and CloudSat observations. *Remote Sensing of the Atmosphere, Clouds, and Precipitation*, E. Im, S. Yang, and P. Zhang, Eds., International Society for Optical Engineering (SPIE Proceedings, Vol. 9259), doi:10.1117/12.2069110, 2014.

755 Wang, W., Huang, J., Minnis, P., Hu, Y., Li, J., Huang, Z., Ayers, J. K., and Wang, T.: Dusty cloud properties and radiative forcing over dust source and downwind regions derived from A-Train data during the Pacific Dust Experiment, *J. Geophys. Res.*, 115, D00H35, doi:10.1029/2010JD014109, 2010.

760 Weger, R. C., Lee, J., Zhu, T., and Welch, R. M.: Clustering, randomness and regularity in cloud fields: 1. Theoretical considerations, *J. Geophys. Res.*, 97, 20519–20536, doi:10.1029/92JD02038, 1992.

Willén, U., Crewell, S., Baltink, H. K., and Sievers, O.: Assessing model predicted vertical cloud structure and cloud overlap with radar and lidar ceilometer observations for the Baltex Bridge Campaign of CLIWA-NET, *Atmos. Res.*, 75(3), 227-255, 2005.

765 Winker, D. M., Hunt, W. H. and McGill, M. J.: Initial performance assessment of CALIOP, *Geophys. Res. Lett.*, 34(19), 228-262, 2007.

Wu, G., Duan, A., Liu, Y., Mao, J., Ren, R., Bao, Q., He, B., Liu, B., and Hu, W.: Tibetan Plateau climate dynamics: recent research progress and outlook, *National Science Review*, 2(1), 100-116, 2015.

770 Wu, G. X., Liu, Y., Wang, T., Wan, R., Liu, X., Li, W., Wang, Z., Zhang, Q., Duan, A., and Liang X.: The influence of the mechanical and thermal forcing of the Tibetan Plateau on the Asian climate, *J. Hydrometeorol.*, 8, 770–789, doi:10.1175/JHM609.1, 2007.

775 Wu, H., Yang, K., Niu, X., and Chen, Y.: The role of cloud height and warming in the decadal weakening of atmospheric heat source over the Tibetan Plateau, *Sci. China Ser. D.*, 58(3), 395–403, doi:10.1007/s11430-014-4973-6, 2015.

Xu, X., Lu, C., Shi, X., and Gao, S.: World water tower: An atmospheric perspective, *Geophys. Res. Lett.*, 35(20), 525-530, 2008.

780 Yan, H.R., Li, Z.Q., Huang, J.P., Cribb, M., Liu, J.J.: Long-term aerosol-mediated changes in cloud radiative forcing of deep clouds at the top and bottom of the atmosphere over the Southern Great Plains, *Atmos. Chem. Phys.*, 14(14), 7113-7124, 2014.

Yan, Y., Liu, Y. and Lu, J.: Cloud vertical structure, precipitation, and cloud radiative effects over Tibetan Plateau and its neighboring regions, *J. Geophys. Res. Atmos.*, 121 (2016), pp. 5864-5877, doi:10.1002/2015JD024591, 2016.

- Yanai, M., Li, C. F., and Song, Z. S.: Seasonal heating of the Tibetan Plateau and its effects on the evolution of the Asian summer monsoon, *J. Meteor. Soc. Japan*, 70, 319–351, 1992.
- Yang, K., Wu, H., Qin, J., Lin, C., Tang, W., and Chen, Y.: Recent climate changes over the Tibetan Plateau and their impacts on energy and water cycle: A review, *Global and Planetary Change*, 112(1), 79-91, 2014.
- Yang, K., Ding B., Qin, J., Tang W., Lu, N., and Lin, C.: Can aerosol loading explain the solar dimming over the Tibetan Plateau?, *Geophys. Res. Lett.*, 39, L20710, doi: 10.1029/2012GL053733, 2012.
- Yang, K., Guo, X., He, J., Qin, J. and Koike, T.: On the climatology and trend of the atmospheric heat source over the Tibetan Plateau: an experiments-supported revisit, *J. Clim.*, 24, 1525 – 1541, 2011.
- Yoo, H., Li, Z., You, Y., Lord, S., Weng F, and Barker H. W.: Diagnosis and testing of low-level cloud parameterizations for the NCEP/GFS model satellite and ground-based measurements, *Clim. Dyn.*, 41(5-6), 1595-1613, doi:10.1007/s00382-013-1884-8, 2013.
- You, Q., Jiao, Y., Lin, H., Min, J., Kang, S., Ren, G., and Meng, X.: Comparison of NCEP/NCAR and ERA-40 total cloud cover with surface observations over the Tibetan Plateau, *International Journal of Climatology*, 34(8), 2529-2537, 2014.
- Yuan, T., and Oreopoulos, L.: On the global character of overlap between low and high clouds, *Geophys. Res. Lett.*, 40, 5320-5326, 2013.
- Zhang, H., and Jing, X.: Advances in studies of cloud overlap and its radiative transfer in climate models, *J. Meteoro. Res.*, 30(2), 156-168, 2016.
- Zhang, H., Peng, J., Jing, X., and Li, J.: The features of cloud overlapping in Eastern Asia and their effect on cloud radiative forcing, *Science China Earth Sciences*, 56(5), 737-747, 2013.
- Zhang, H., and Jing, X. W.: Effect of cloud overlap assumptions in climate models on modeled earth-atmophere radiative fields, *Chinese Journal of Atmospheric Sciences*, 34(3), 520-532, 2010.
- Zhao, C.F., Liu, L.P., Wang, Q.Q., Qiu, Y.M., Wang, Y., and Wu, X. L.: MMCR-based characteristic properties of non-precipitating cloud liquid droplets at Naqu site over Tibetan Plateau in July 2014, *Atmospheric research*, 190, 68-76, doi.org/10.1016/j.atmosres.2017.02.002, 2017.
- Zhao, C.F., Liu, L.P., Wang, Q.Q., Qiu, Y.M., Wang, W., Wang, Y., and Fan, T.Y.: Toward Understanding the Properties of High Ice Clouds at the Naqu Site on the Tibetan Plateau Using Ground-Based Active Remote Sensing Measurements Obtained during a Short Period in July 2014, *Journal of Applied Meteorology and Climatology*, 55, 2493-2507, doi:10.1175/JAMC-D-16-0038.1, 2016.
- Zhu, L., Xie, M. and Wu, Y.: Quantitative analysis of lake area variations and the influence factors from 1971 to 2004 in the Nam Co basin of the Tibetan Plateau, *Chin. Sci. Bull.* 55, 1294 – 1303, 2010.

Table 1. Parameterizations of decorrelation scale length L from the exponential fit as a function of atmospheric stability $\partial\theta_{es}/\partial z$, wind shear dV/dz or latitude Φ

Scheme	description	decorrelation length scale L
Wind shear (Di Giuseppe and Tompkins, 2015)	Random/Maximum, only wind shear	$L = 4.4 - 0.45 \times \frac{dV}{dz}$
Wind shear (this study)	Random/Maximum, only wind shear	$L = 2.19 - 0.14 \times \frac{dV}{dz}$
Wind shear-instability (this study)	Random/Maximum, wind shear and instability	$L = 2.18 - 0.09 \times \frac{dV}{dz} - 0.15 \times \frac{\partial\theta_{es}}{dz}$
Latitude (Shonk et al., 2010)	Random/Maximum, only latitude	$L = 2.899 - 0.02759 \times \Phi $

830

Figure Captions

Figure 1. (a) CloudSat overpass tracks (blue line: daytime; red line: nighttime) over the Tibetan Plateau (27 N-39 N; 78 E-103 E); (b) A sample of CloudSat 2B-GEOPROF-LIDAR cloud mask product along the ground track of 200km (white color: cloud fraction>99%; light blue: 0<cloud fraction<99%; deep blue: clear sky; orange color: surface). (c) The observed and calculated segment-average cloud covers profiles based on maximum and random assumptions for different spatial scales and given cloud mask sample in Fig. 1b. (d) The corresponding cloud overlap parameters of continuous cloud pair for 25, 50, 100 and 200 km spatial scale. Note that the observations below 1 km over the TP surface have been removed.

Figure 2. The dependence of α on the layer separation and its sensitivity to the spatial scale for (a) non-continuous and (b) continuous cloud pairs; the error bars

correspond to ± 3 standard error; (c) The probability distribution functions (PDFs) of the along-track horizontal scales of cloud system at different height over TP region; (d) The variations of cloud sample numbers and the cumulative percentages with cloud
850 layer separations for both non-continuous and continuous clouds at a given spatial scale of 50km. The cumulative percentages represent the proportions of cloud sample below corresponding layer separation to all samples.

Figure 3. The monthly variations of the pentad-averaged (a) cloud overlap parameter, α , (c) conditional instability to moist convection, $\partial\theta_{es}/\partial z$, (e) wind shear, dV/dz , (g) and vertical velocity at 500 hPa, ω for the continuous clouds over the TP ; The
855 monthly variations of the pentad-averaged (b) α , (d) $\partial\theta_{es}/\partial z$, (f) dV/dz and (h) ω for the continuous clouds for the layer separation of 2 km (red) and 3km (black).

Figure 4. The zonal variations of the (a) α , (c) $\partial\theta_{es}/\partial z$, (e) dV/dz , and (g) ω for the continuous clouds over the TP ; The zonal variations of the (b) α , (d) $\partial\theta_{es}/\partial z$, (f) dV/dz and (h) ω for the continuous clouds for the layer separation of 2 km (red) and 3km (black).
860

Figure 5. The sensitivities of median overlap parameter α to (a) wind shear, (b) instability and (c) vertical velocity at 500 hPa at given upper limit of cloud cover (50%) and spatial scale (50 km) for the continuous clouds. The error bars correspond to ± 3 standard error.
865

Figure 6. The monthly differences in cloud cover between calculation and observation for different schemes (see the Table 1) and its dependence on the layer separation.
870

Figure 7. The zonal differences in cloud cover between calculation and observation for different schemes (see the Table 1) and its dependence on the layer separation.
875

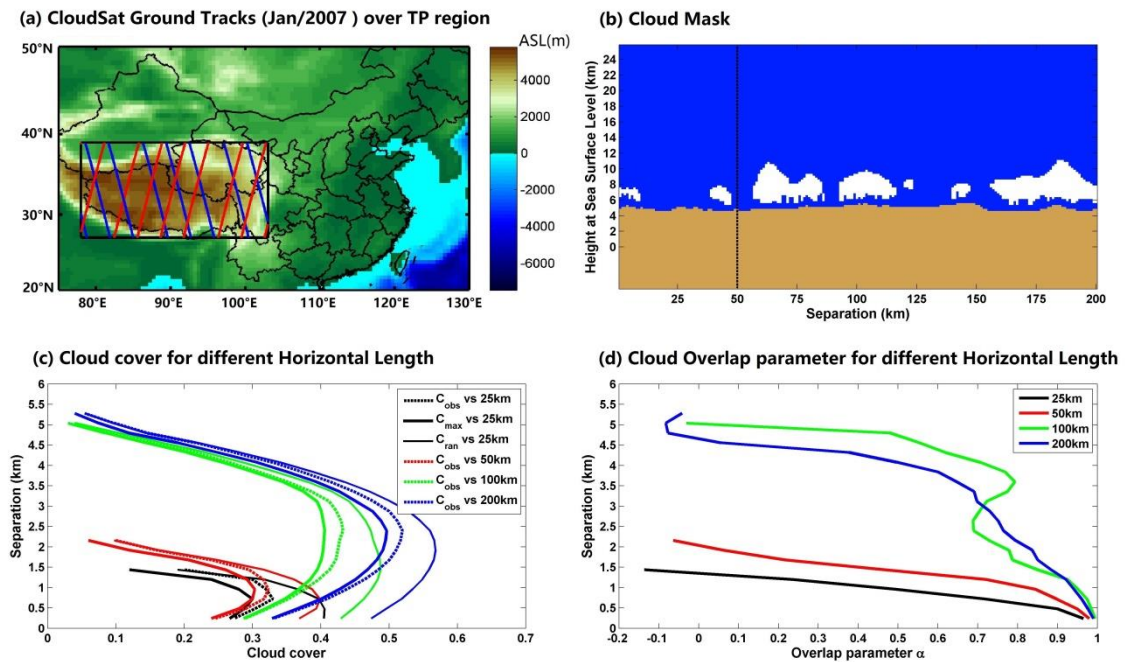


Figure 1. (a) CloudSat overpass tracks (blue line: daytime; red line: nighttime) over the Tibetan Plateau (27°N-39°N; 78°E-103°E); (b) A sample of CloudSat 2B-GEOPROF-LIDAR cloud mask product along the ground track of 200km (white color: cloud fraction > 99%; light blue: 0 < cloud fraction < 99%; deep blue: clear sky; orange color: surface). (c) The observed and calculated segment-average cloud covers profiles based on maximum and random assumptions for different spatial scales and given cloud mask sample in Fig. 1b. (d) The corresponding cloud overlap parameters of continuous cloud pair for 25, 50, 100 and 200 km spatial scale. Note that the observations below 1 km over the TP surface have been removed.

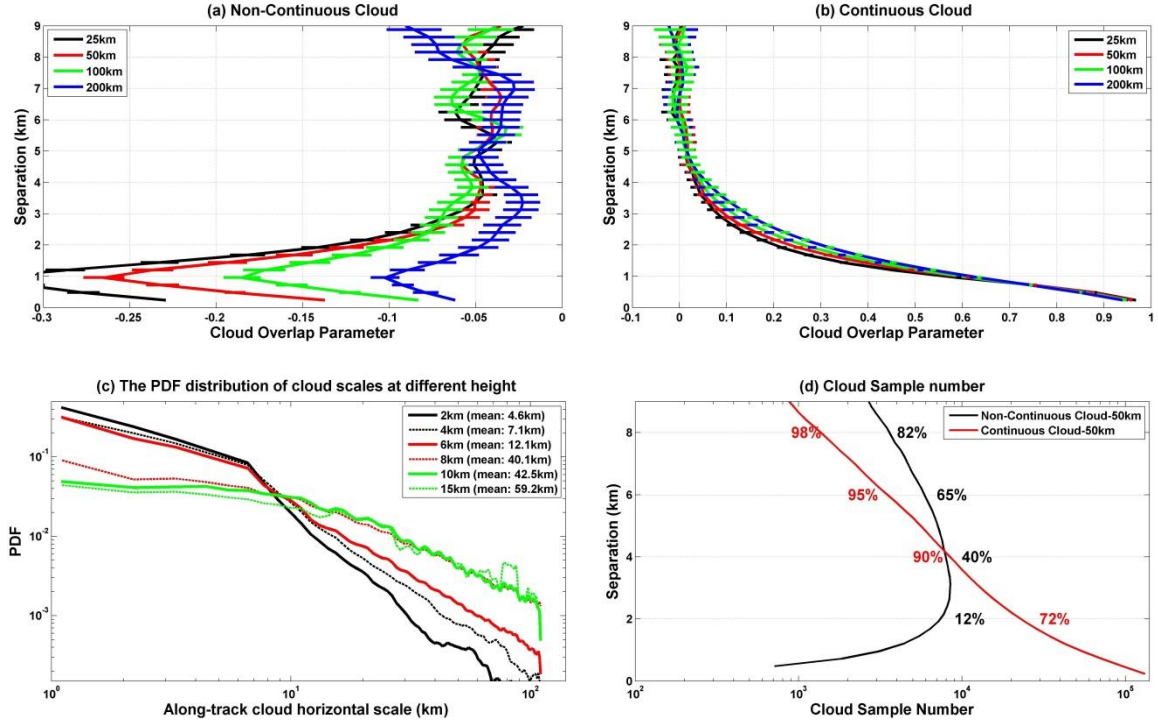


Figure 2. The dependence of α on the layer separation and its sensitivity to the spatial scale for (a) non-continuous and (b) continuous cloud pairs; the error bars correspond to ± 3 standard error; (c) The probability distribution functions (PDFs) of the along-track horizontal scales of cloud system at different height over TP region; (d) The variations of cloud sample numbers and the cumulative percentages with cloud layer separations for both non-continuous and continuous clouds at a given spatial scale of 50km. The cumulative percentages represent the proportions of cloud sample below corresponding layer separation to all samples.

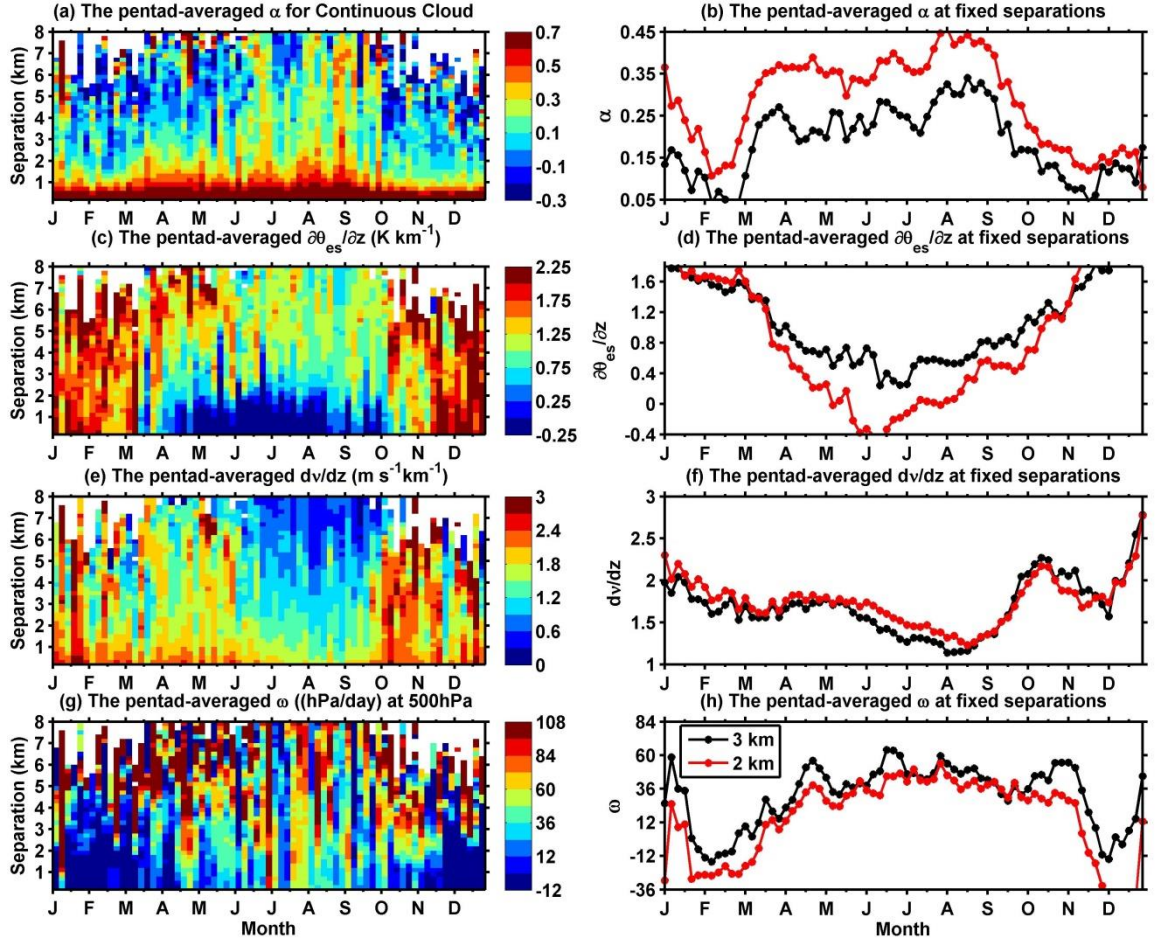


Figure 3. The monthly variations of the pentad-averaged (a) cloud overlap parameter, α , (c) conditional instability to moist convection, $\partial\theta_{es}/\partial z$, (e) wind shear, dV/dz , (g) and vertical velocity at 500 hPa, ω for the continuous clouds over the TP ; The monthly variations of the pentad-averaged (b) α , (d) $\partial\theta_{es}/\partial z$, (f) dV/dz and (h) ω for the continuous clouds for the layer separation of 2 km (red) and 3km (black).

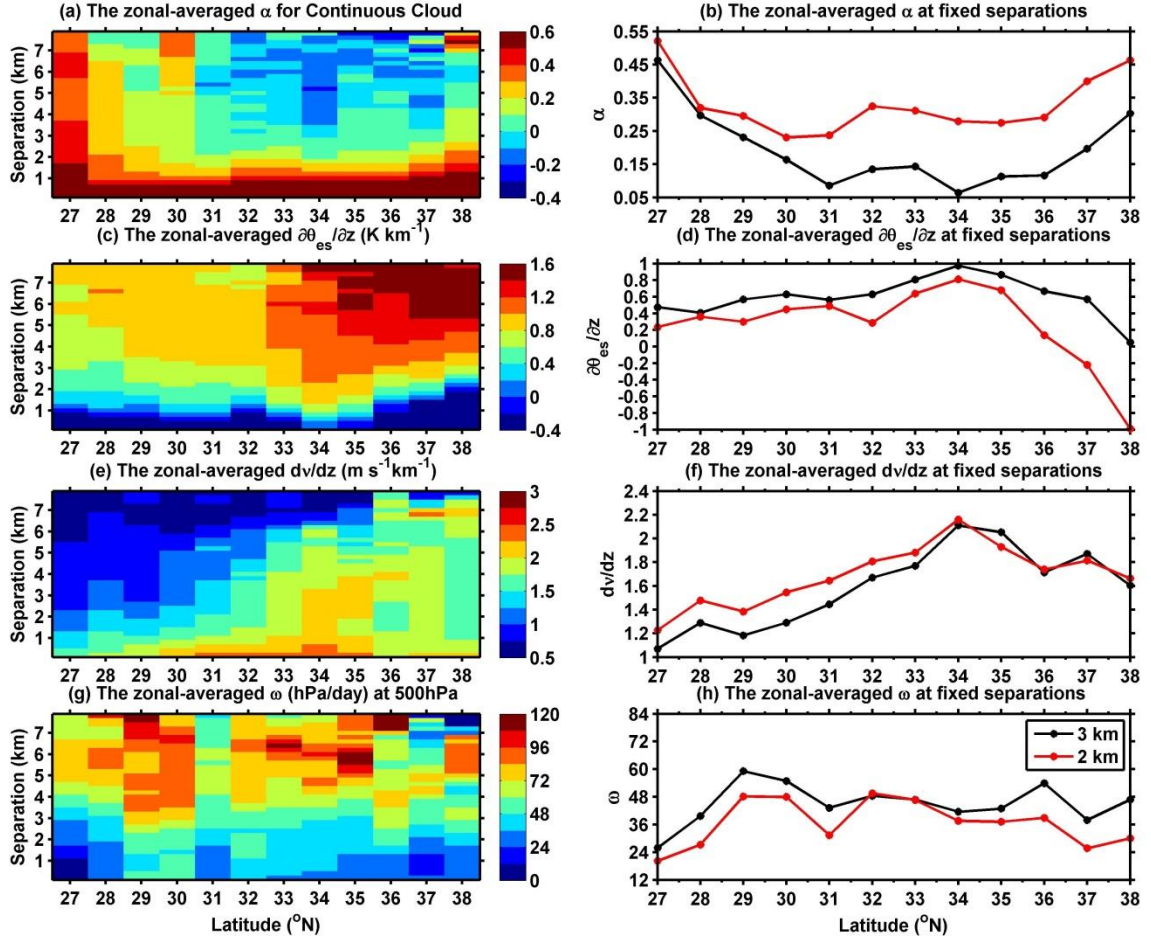


Figure 4. The zonal variations of the (a) α , (c) $\partial\theta_{es}/\partial z$, (e) dV/dz , and (g) ω for the continuous clouds over the TP; The zonal variations of the (b) α , (d) $\partial\theta_{es}/\partial z$, (f) dV/dz and (h) ω for the continuous clouds for the layer separation of 2 km (red) and 3km (black).

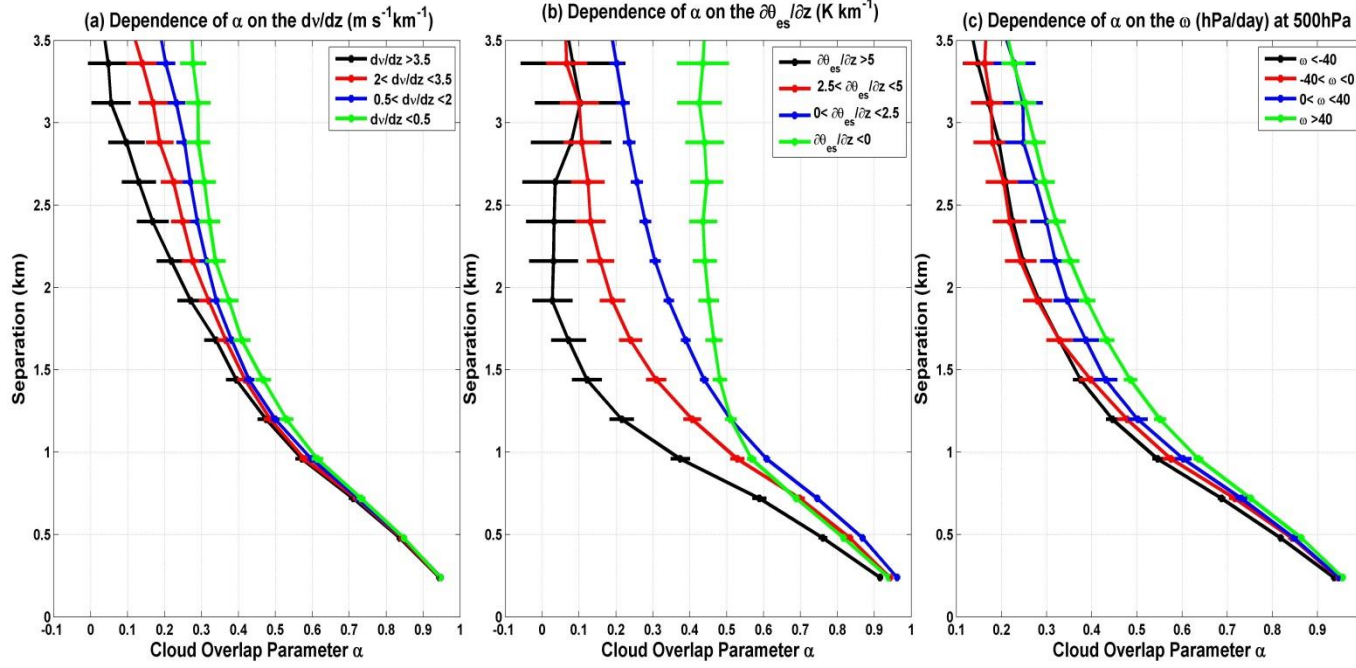


Figure 5. The sensitivities of median overlap parameter α to (a) wind shear, (b) instability and (c) vertical velocity at 500 hPa at given upper limit of cloud cover (50%) and spatial scale (50 km) for the continuous clouds. The error bars correspond to ± 3 standard error.

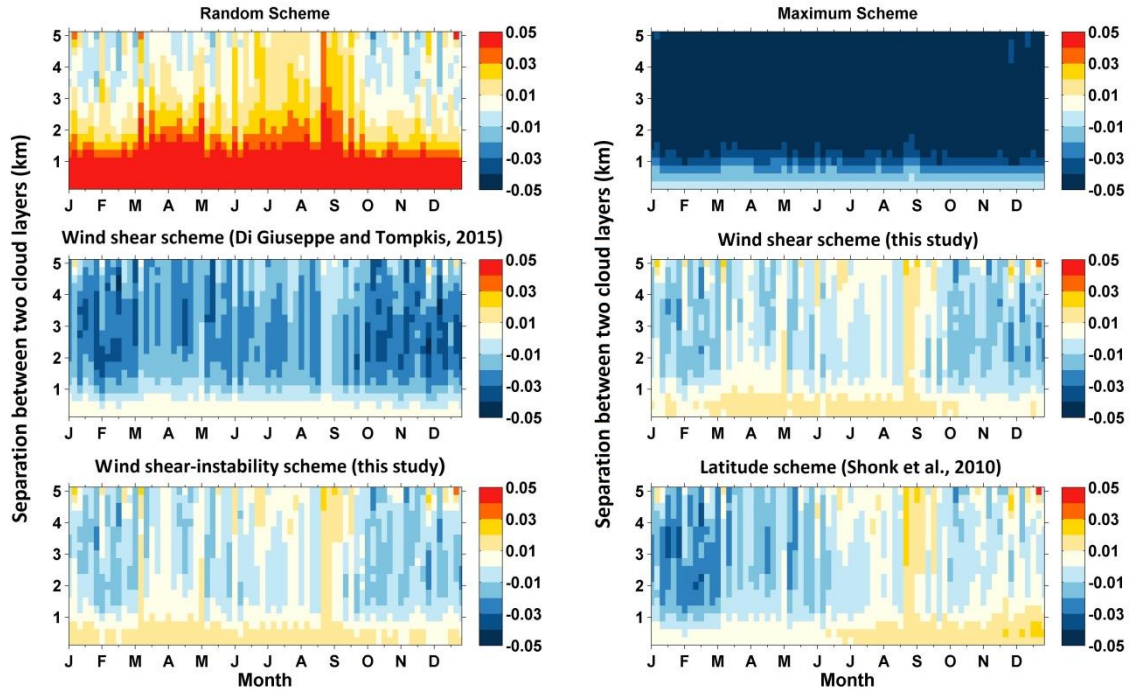


Figure 6. The monthly differences in cloud cover between calculation and observation
 940 for different schemes (see the Table 1) and its dependence on the layer separation.

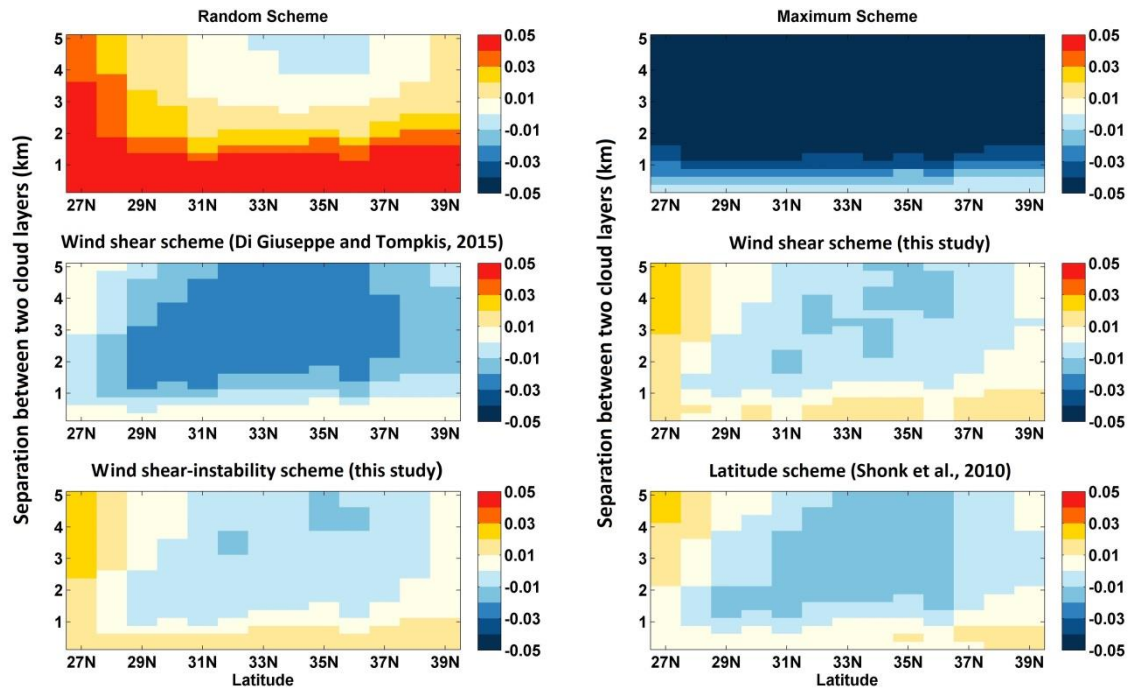


Figure 7. The zonal differences in cloud cover between calculation and observation
 945 for different schemes (see the Table 1) and its dependence on the layer separation.